Generation of milliCharged particles at the LHC

C. Campagnari, B. Marsh (UCSB), F. Golf (UNL)

May 6, 2020

1 Introduction

We discuss the MC generation of milliCharged particles (χ) in pp collisions at the LHC in the central rapidity region. Except for Drell-Yan (DY), this is done in a few steps

1. Generate in various ways SM particles (A) that can decay as $A \to X\chi^+\chi^-$

2. Keep track of the cross-section for SM production of A.

3. Calculate the branching ratio for $A \to X\chi^+\chi^-$ for milliCharge $Q = 1$. For different charges, it is easy to scale the branching ratio as Q^2.

4. Generate the $A \to X\chi^+\chi^-$ decay with proper kinematics.

5. Save the "event" for further processing in a root file.

2 Special (simplest) case: Drell-Yan

The Drell-Yan process $pp \to \chi^+\chi^-$ is generated with the external model interface in Mad-Graph. Note that we cannot use SM $pp \to \ell^+\ell^-$ with a different lepton mass because the couplings of the Z to χs and leptons are different (in our model χs are weak isospin singlets[1][2]).

Technically, this was achieved in MadGraph by simply modifying the mass and couplings of the SM electron. The couplings are εe and $-\varepsilon e \tan\theta_W$ to the γ and Z_0, respectively, where $\varepsilon = Q/e$.

The $pp \to \chi^+\chi^-$ process is generated with up to 1 extra parton. This is not very relevant at lower masses since a large majority of events don't include an extra parton. At higher masses, however, it can increase cross section by $O(20\text{-}30\%)$. The MadGraph parameter `xqcut` is set to 0, but there still seems to be a 20 GeV cut on the p_T of the extra parton.

We can't find a parameter to control this, but there appears to be a $\chi^+\chi^-$ invariant mass cut of 2 GeV. Correspondingly, the cross section plateaus below $m_\chi = 1$ GeV. This shouldn't matter, however, as production from J/ψ, ϕ, ω, ρ, etc. is expected do dominate at low masses.

A plot of DY cross section as a function of mass is shown along with the other production modes in Fig. 8. Note that DY is handled specially here: while for the other modes we require

the mother particle to have $|\eta| < 2$, this does not make sense for DY (unless there is an extra parton produced, the η of the "mother" is $\pm\infty$). Instead we have required at least one mCP to have $|\eta| < 1$. This threshold was chosen so that the probability of an mCP pointing in the vicinity of the detector is similar between DY and the other modes, in order to facilitate comparison of cross sections.

3 List of non-DY processes

The main processes for $A \to e^+ e^- X$ at the LHC are:

- $\pi^0 \to e^+ e^- \gamma$ (BR=1.17%, Dalitz decay)

- $\eta \to e^+ e^- \gamma$ (BR=0.7%, Dalitz decay)

- $\eta' \to e^+ e^- \gamma$ (BR=5e-4, Dalitz decay)

- $\omega \to \pi^0 e^+ e^-$ (BR=8e-4, Dalitz decay)

- $\eta' \to \omega e^+ e^-$ (BR=2e-4, Dalitz decay)

- $\eta' \to \pi^+ \pi^- e^+ e^-$ (BR=2e-3, skip, see comment in Section 6)

- $V \to e^+ e^-$ (V = onia, ϕ, ρ, ω)

Note that if we are only interested in χ masses above 100 MeV, Dalitz decays of π^0 and decays of η' into ω do not contribute. In all cases the BR for $A \to \chi^+ \chi^- X$ can be obtained by rescaling $A \to e^+ e^- X$ by a factor of Q^2 times an additional mass-dependent factor. In general this factor consists of a phase space piece $\sqrt{1 - (2m_\chi/m_A)^2}$ plus an additional piece that arises from the matrix element.

Note also that among these processes, the paper [2] that proposed the milliqan experiment only included onia. Furthermore it is not clear that it included the $B \to \psi$ process, it is not clear that it included $\psi(2S)$, $\Upsilon(2S)$, and $\Upsilon(3S)$, and it imposed requirements $p_T > 6.5$ GeV (2 GeV) on J/ψ and $\Upsilon(1S)$, respectively. The Letter of Intent [3] also mentions $\Upsilon(2S)$ and $\Upsilon(3S)$, and it is possible that the latest NSF proposal included even more processes. In any case: here we make an attempt to include as many processes as possible and to remove p_T requirements.

4 Branching Ratios of non-DY processes (Q=1).

4.1 Dalitz BR

The partial width for $A \to e^+ e^- \gamma$ can be written as[4, 5]:

$$\frac{d\Gamma}{dq^2} = \frac{2\alpha}{3\pi q^2} \ (1 + \frac{2m_e^2}{q^2}) \ \sqrt{1 - \frac{4m_e^2}{q^2}} \ (1 - \frac{q^2}{m_A^2})^3 \ |F(q^2)|^2 \ \Gamma(A \to \gamma\gamma) \tag{1}$$

2

m_χ (MeV)	$\pi^0 \to \chi\chi\gamma$	$\eta \to \chi\chi\gamma$	$\eta' \to \chi\chi\gamma$	$\eta' \to \chi\chi\omega$	$\omega \to \chi\chi\pi^0$
0.511 ($=m_e$)	1.17 e-2	6.6 e-3	4.6 e-4	1.8 e-4	7.6 e-4
PDG for ee	(1.17 ± 0.04)e-2	(6.9 ± 0.4)e-4	(4.7 ± 0.3)e-4	(2.0 ± 0.4)e-4	(7.7 ± 0.6)e-4
10	2.8 e-3	2.9 e-3	2.5 e-4	5.7 e-5	3.7 e-4
30	3.5 e-4	1.6 e-3	1.8 e-4	1.7 e-5	2.3 e-4
50	1.2 e-5	1.0 e-3	1.4 e-4	4.3 e-6	1.6 e-4
60	2.7 e-7	8.2 e-4	1.3 e-4	1.7 e-6	1.4 e-4
90		4.3 e-4	1.0 e-4		9.2 e-5
105.7 ($=m_\mu$)		3.0 e-4	9.2 e-5		7.4 e-5
PDG for $\mu\mu$		(3.1 ± 0.4) e-4	(1.1 ± 0.3) e-4		(1.3 ± 0.2) e-4
150		8.9 e-5	6.8 e-5		3.7 e-5
200		1.2 e-5	4.8 e-5		1.5 e-5
250		1.0 e-7	3.2 e-5		3.6 e-6
400			5.6 e-7		

Table 1: Branching ratios for different Dalitz decay modes as a function of m_χ for $Q = 1$ calculated based on equations 1, 2, and 3. When possible we compare with the values from the 2019 PDG.

where m_A is the mass of A, q^2 is the mass-squared of the e^+e^- pair, and $F(q^2)$ is a form factor. Note the $1/q^2$ factor that results in a highly non-uniform invariant mass distribution sharply peaked at low values. The form factor is such that $F(0) = 1$ and for pions is usually parametrized near $q^2 = 0$ as $F(q^2) = 1 + a\frac{q^2}{m_\pi^2}$ with $a \approx 0.03$. The form factor can also be estimated in the Vector Dominance Model (VDM) as

$$|F(q^2)|^2 = \frac{m_\rho^4 + m_\rho^2\Gamma_\rho^2}{(m_\rho^2 - q^2)^2 + m_\rho^2\Gamma_\rho^2} \tag{2}$$

where m_ρ and Γ_ρ are the mass and width of the ρ meson. The VDM model assumes that the decay proceeds through $\pi^0 \to \gamma V^*, V^* \to e^+e^-$ and $V = \rho$ or ω; equation 2 neglects the difference between ρ and ω.

In the case of $A \to e^+e^-X$, when X is not γ, the partial width can be written as

$$\frac{d\Gamma}{dq^2} = \frac{\alpha}{3\pi q^2} \left(1 + \frac{2m_e^2}{q^2}\right) \sqrt{1 - \frac{4m_e^2}{q^2}} \cdot$$
$$\left[\left(1 + \frac{q^2}{m_A^2 - m_X^2}\right)^2 - \frac{4m_A^2 q^2}{(m_A^2 - m_X^2)^2}\right]^{3/2} |F_{AX}(q^2)|^2 \ \Gamma(A \to X\gamma) \tag{3}$$

where m_X is the mass of X, and the transition form factor F_{AX} can also be approximated as in equation 2.

For milliCharged particles, Dalitz decays branching ratios can be obtained by integrating equation 1 or 3 from $q^2 = 4m_\chi^2$ to the kinematical limit, substituting m_χ for m_e, and rescaling by Q^2. Some numerical results for $Q = 1$ are given in Table 1. Note the sharp drop in branching ratios with mass. This is due to the $1/q^2$ behavior. The calculations with the electron and muon masses are in excellent agreement with the PDG.

Decay mode	PDG BR value	Calculation
$\Upsilon(1S) \to \tau\tau$	(2.6 ± 0.1)e-2	(2.4 ± 0.1)e-2
$\psi(2S) \to \tau\tau$	(3.1 ± 0.4)e-3	(3.1 ± 0.0)e-3
$\phi \to \mu\mu$	(2.9 ± 0.2)e-4	(3.0 ± 0.0)e-4
$\omega \to \mu\mu$	(7.4 ± 1.8)e-5	(7.3 ± 0.2)e-5
$\rho \to \mu\mu$	(4.6 ± 0.3)e-5	(4.7 ± 0.1)e-5

Table 2: Comparison of the PDG and calculated values od the $V \to \ell\ell$ branching ratios. The quoted uncertainty on the calculation reflects the uncertainty on the $V \to ee$ branching ratio.

4.2 Vector meson branching ratios

At lowest order the SM decay rate for $V \to \ell\ell$ is given by the Van Royen-Weisskopf formula[6, 7]:

$$\Gamma(V \to \ell\ell) = 4\pi\alpha^2 \frac{f_V^2}{m_V} Q_q^2 (1 - 4x_\ell^2)^{1/2}(1 + 2x_\ell^2) \tag{4}$$

where f_V is the vector decay constant, m_V is the vector mass, Q_q is the charge of the quark that makes up the meson, $x_\ell = m_\ell/m_V$, and m_ℓ is the lepton mass.

Thus the ratio of BR for $V \to \chi\chi$ to $V \to ee$ is given by

$$\frac{\Gamma(V \to \chi\chi)}{\Gamma(V \to ee)} = Q^2 \frac{(1 - 4x_\chi^2)^{1/2}(1 + 2x_\chi^2)}{(1 - 4x_\ell^2)^{1/2}(1 + 2x_\ell^2)} \tag{5}$$

where $x_\chi = m_\chi/m_V$, and m_χ is the mass of χ.

As a sanity check, we use equation 5 to predict several $V \to \ell\ell$ branching ratios and compare them with their PDG values, see Table 2. To be fair the tests with $\ell = \mu$ are not very powerful since $x_\mu^2 \approx x_e^2 \approx 0$.

5 Generation of SM particles decaying into $\chi^+\chi^-$

The key features of our approach are the following

- Use theory or published data, or some MC to generate p_T distributions for SM particles saved as histograms in ROOT files (Drell Yan is an exception, as discussed previously).

- Sample the ROOT histograms to generate SM particles of a given p_T.

- Pick azimuthal angles ϕ and pseudorapity η in a limited range, matched to the acceptance of milliqan. The η distribution is assumed to be flat, see comments in Section 6.

- Decay the SM particles into milliCharged particles.

- When possible, keep track of theoretical uncertainties.

- In general it is sufficient to generate SM particles at low and moderate p_T since that is where the cross-section is largest.
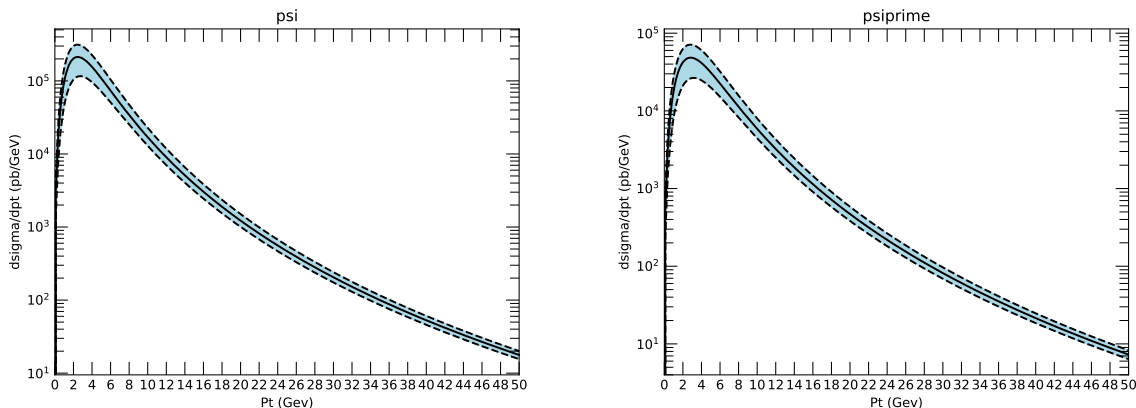
Figure 1: Transverse momentum distributions of J/ψ (left) and ψ' from bottom quark decays. Note: this is from a single b, multiply by two to include $\bar{b}$. The units are pb/GeV and the distributions are integrated over $|\eta| < 1.0$.

5.1 J/ψ and ψ' from b-decays

We use the tool available in

http://www.lpthe.jussieu.fr/ cacciari/fonll/fonllform.html

to generate histograms of p_T distributions (cross-sections) for charmonium from bottom decays, including theoretical uncertainties[9, 10]. See Figure 1

5.2 Direct onia production

5.2.1 Direct bottonium

There have been many measurement of the p_T spectra od Υ in pp collisions at the LHC by CMS [11, 12, 13, 14], Atlas [15, 16], and LHCb [17, 18, 19, 20, 21]. The LHCb measurements are in the forward region. The only measurement at 13 TeV in the central region is from CMS [14]. Unfortunately, it is limited to $p_T > 20$ GeV.

Due to the lack of 13 TeV data, initially we planned to use theoretical predictions as a basis of the Υ event generation. We contacted the theorists [22] that provided the state-of-the art calculations used to confront the data in Reference [14]. We asked them to extend their predictions to lower p_T, unfortunately they claim that these are unreliable below 15 GeV.

As a result we decided to use 7 TeV data for $p_T < 20$ GeV and the CMS 13 TeV data at higher p_T. A key ingredient is the ratio of 13 and 7 GeV Υ production cross-sections. These have been measured for $p_T > 20$ GeV and $|\eta| < 1.2$ by CMS, see Figure 2 of Reference [14]. The ratios are about 1.7 at $p_T = 20$ GeV, irrespective of Υ state (1S, 2S, or 3S), and increase slowly to about 2 at $p_T = 40$ GeV. The ratios have also been measured by LHCb [17] all the way down to zero p_T for $2.0 < y < 2.5$, see Figure 2. The LHCb ratios in the 20-30 GeV region measured at slightly higher y are in agreement with the more central ratios measured by CMS.
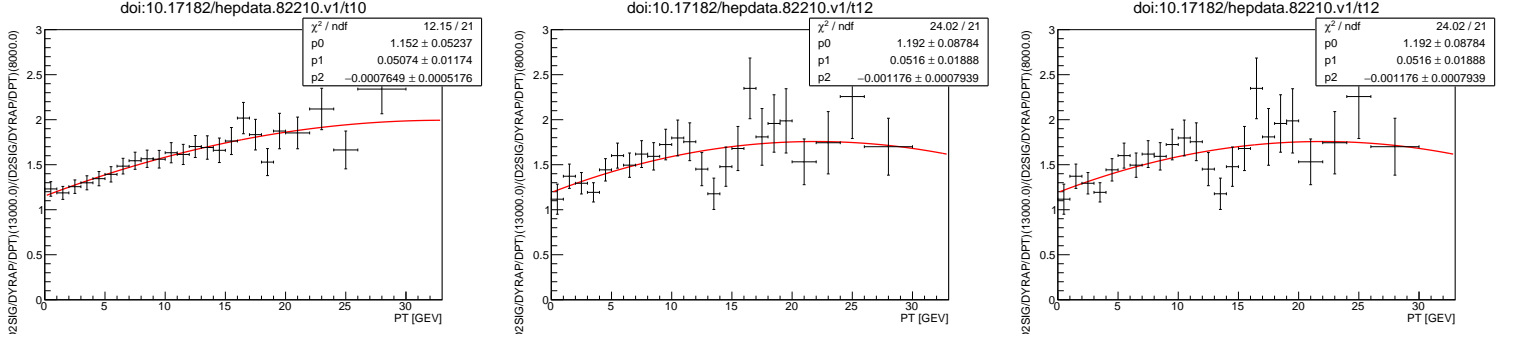
Figure 2: Ratio of 13 to 7 GeV Υ cross-section for $2.0 < y < 2.5$ from LHCb [17]. From left to right: 1S, 2S, 3S. The quadratic fits are ours.
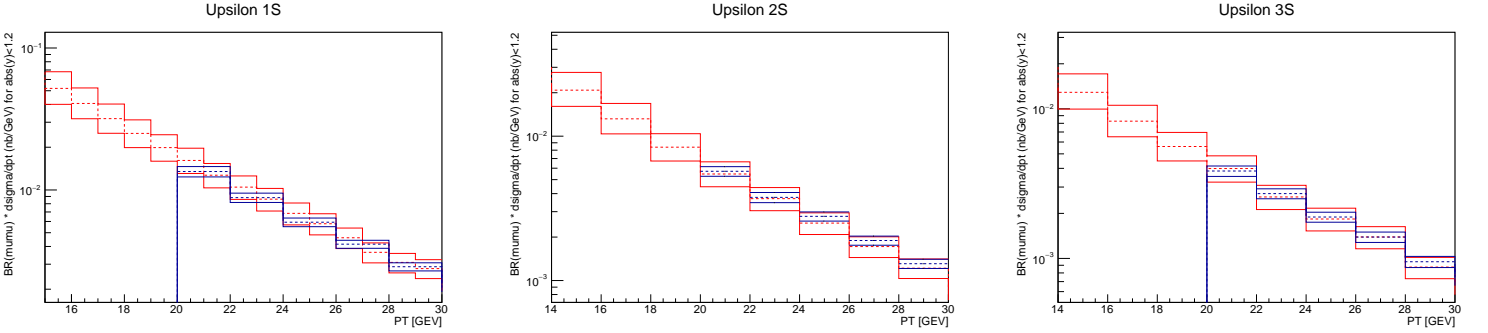

Figure 3: Comparison of the rescaled 7 GeV Atlas Υ spectra (red) with the 13 GeV CMS spectra (blue) in the neighborhood of 20 GeV, where the matching of the two spectra takes place. From left to right: 1S, 2S, 3S. The dashed lines represent the central values, the solid lines cover the uncertainty range. This is $\mathcal{B}(\Upsilon \to \mu\mu) \cdot \mathrm{d}\sigma/\mathrm{dp_T}$ in nb/GeV integrated over $|\eta| < 1.2$.
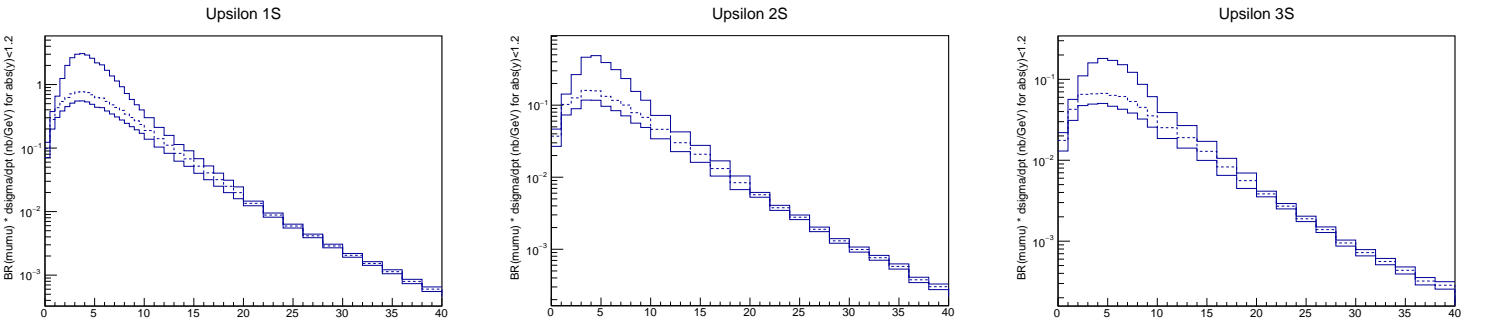

Figure 4: Combined Atlas 7 TeV, CMS 13 TeV Υ spectra. From left to right: 1S, 2S, 3S. The dashed line represent the central value, the solid lines cover the uncertainty range. This is $\mathcal{B}(\Upsilon \to \mu\mu) \cdot \mathrm{d}\sigma/\mathrm{dp_T}$ in nb/GeV integrated over $|\eta| < 1.2$.
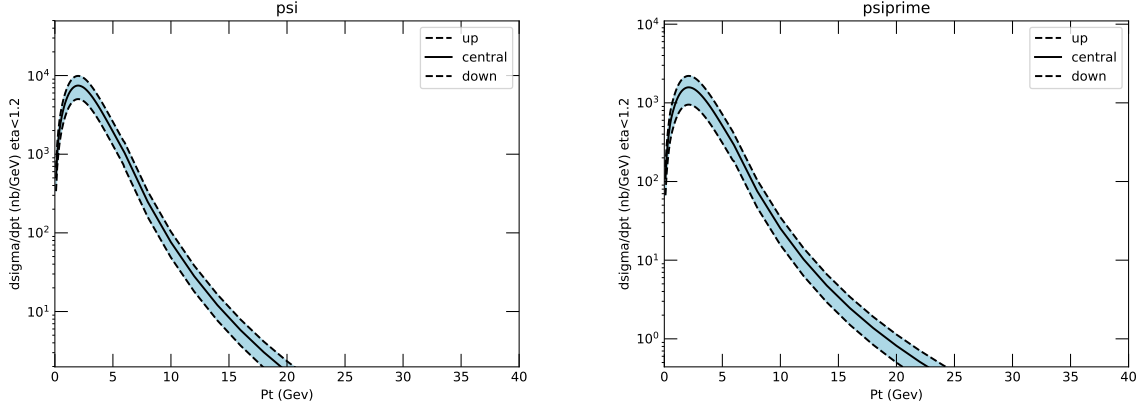
6

Figure 5: Transverse momentum distributions of J/ψ (left) and ψ' from direct production. The units are nb/GeV and the distributions are integrated over $|\eta| < 1.2$.

Consequently, we rescale the **measured** 7 GeV **central** low p_T Υ spectra to 13 TeV using the curves of Figure 2; we combine these with the **measured** 13 TeV **central** high p_T spectra to obtain an inclusive 13 TeV spectra. The 7 TeV data is from Atlas [16], since it happens to be in a more convenient format than the equivalent CMS data. On the other hand the 13 TeV spectra are from CMS [14], since there is no Atlas measurement at 13 TeV.

We demonstrate in Figure 3 that the matching of the Atlas and CMS cross-sections works well. The combined spectra to be used in the event generation are in Figure 4.

5.2.2 Direct charmonium

We take the charmonium spectra from theory [23, 25, 24] see Figure 5.

5.3 J/ψ sanity check

Most of the J/ψ cross-section is from direct production, see Figure 6, left. As a sanity check we also show the fractions of J/ψ and ψ' from b decays measured at lower energy, see Figure 6, right[26].

5.4 π^0, η, η', ϕ, ρ, and ω

We generate these from PYTHIA. The measurement of the $\pi^\pm$ p_T spectrum from CMS[27] is in good agreement with PYTHIA 8 Minimum Bias at low momentum, which gives us some confidence in PYTHIA MinBias. However, we compare PYTHIA to actual measurements of specific particles where possible, to guide the choice of tune and any corrections if necessary.

For π_0's and η's, ALICE measures the differential cross section at 8 TeV and compares to various PYTHIA tunes [31]. The PYTHIA 8 Monash2013 tune [32] predicts π^0's well and η's well until low p_T (<3 GeV), where it overpredicts. So we use the Monash2013 tune and scale down low-p_T η's by a function that grows from 1.0 at 3 GeV to 2.0 at 0.5 GeV.
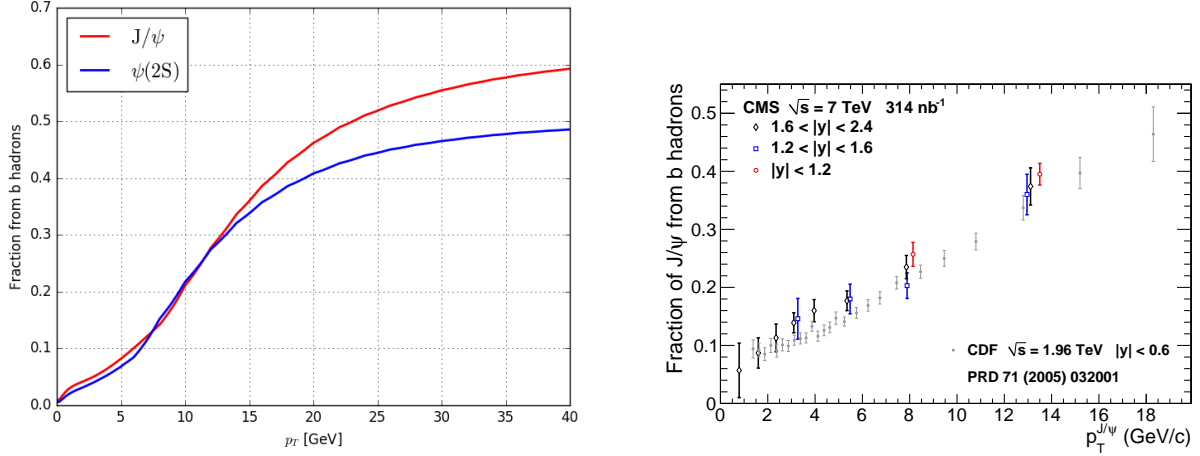
Figure 6: Fraction of charmonium from b decays according to the calculations used in this note (left), and the corresponding measurement (J/ψ only) at lower energy (right). The left plot is for $|\eta| < 1.2$.

For ρ's, ALICE measures the differential cross section at 2.76 TeV [33]. Again Monash2013 agrees well, except at very low p_T (< 1 GeV). So we use this tune, and scale low-p_T ρ's down by a function that grows from 1.0 at 1 GeV to 2.0 at 0.5 GeV.

For ω's, ALICE measures the differential cross section at 7 TeV [34]. Good agreement with Monash2013 is seen everywhere, but the measurement only goes down in p_T to 2 GeV. Since ω production should be similar to ρ production, we use the same low-p_T reweigting scheme as described above.

For ϕ's, ATLAS measures the differential cross section at 7 TeV [35]. Good agreement is seen with the PYTHIA 6 DW tune [36], while the PYTHIA 8 tunes all underpredict. So for ϕ mesons only, we use the PYTHIA 6 DW tune.

To account for observed disagreements with data and variation between tunes, we apply a 30% uncertainty on the production rate for each of these light mesons, uncorrelated across different meson types.

We do not attempt to use QCD $2 \rightarrow 2$ at very low p_T since the process is infrared divergent. PYTHIA `SoftQcd:nonDiffractive` includes all hard QCD processes[28] so in principle this is all that is needed. However, we run out of statistics at high p_T. So at high p_T we stitch together the Min Bias distributions with distributions obtained from QCD $2 \rightarrow 2$ at moderate p_T.

The QCD samples are "p_T-binned", using the `PhaseSpace:pTHat[Min/Max]` parameters in PYTHIA, in bins 15-30 GeV, 30-50 GeV, and 50-80 GeV. The 13 TeV MinBias cross-section is taken to be 80 ± 10 mb (80 mb is the value measured by ATLAS [29] and predicted by PYTHIA, and the 10 mb uncertainty is to account for a 70 mb measurement by CMS [30]). Then the stitching procedure is the following:

- The QCD samples are first normalized to their LO cross-sections.

- Next, we estimate a "QCD-MinBias scale factor" by integrating over some p_T region where the MinBias/QCD ratio is roughly flat.

- The QCD samples are all renormalized by this scale factor.

- The samples are stitched together by visually picking the p_T where the curves cross each other.

The resulting p_T curves are shown in Figure 7. It is not clear what kind of uncertainties we should assign. Eventually we'll have to come up with something (50%?).
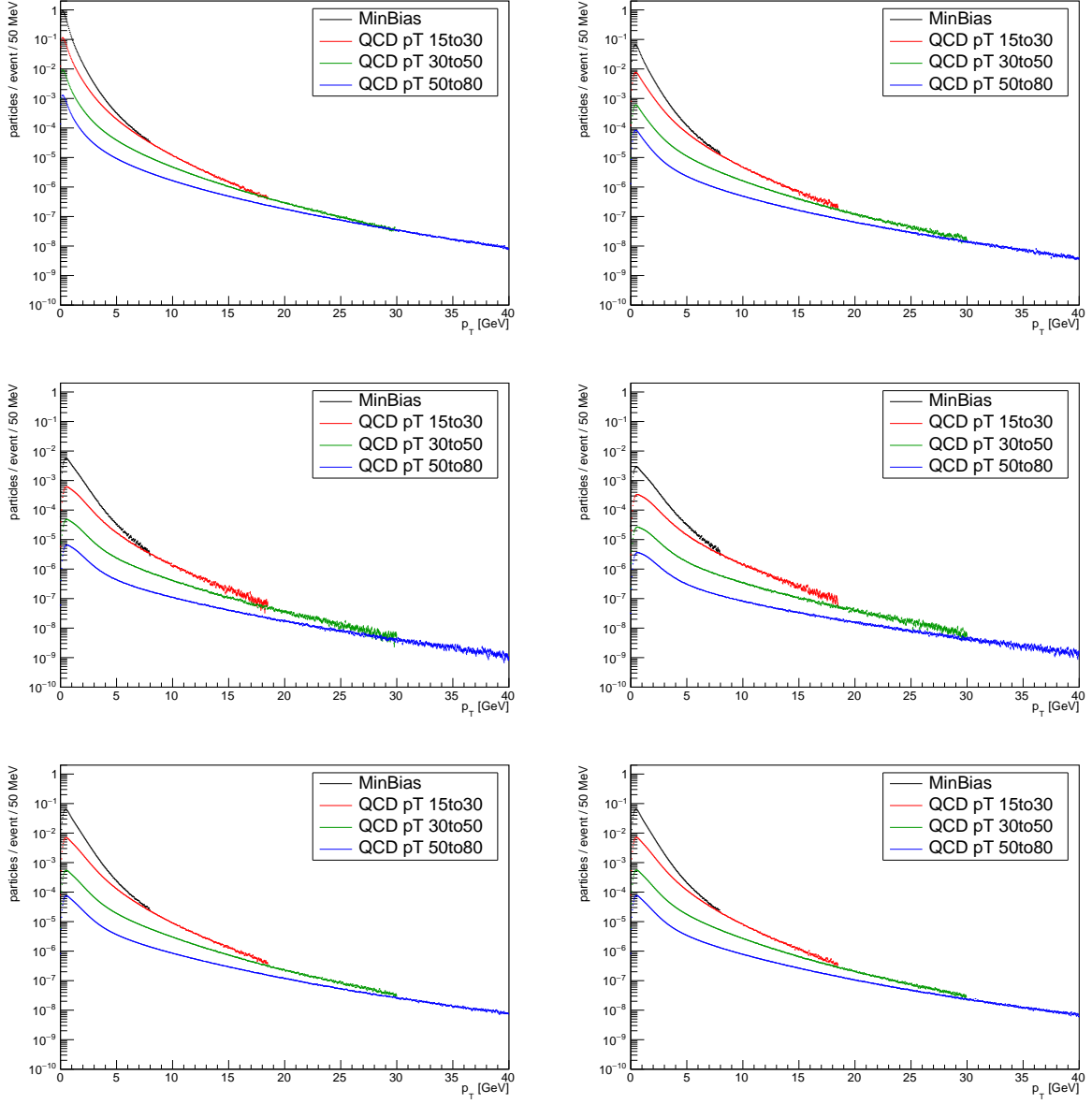
Figure 7: Transverse momentum distributions of π^0, η, η', ϕ, ρ, and ω, top left to bottom right, for $|\eta| < 1$.
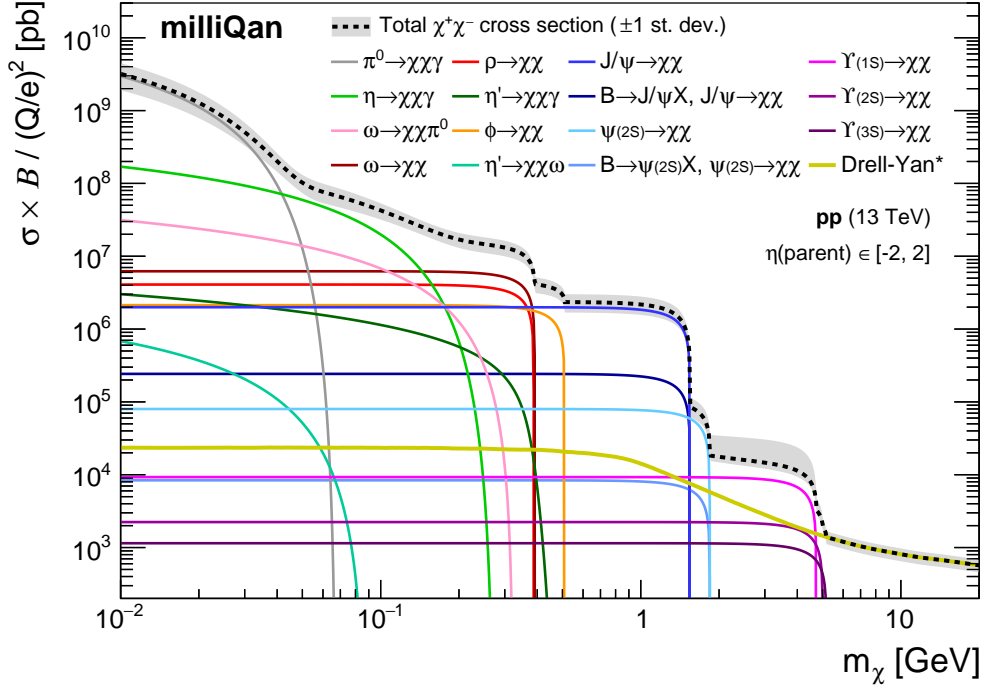
Figure 8: Cross-section times branching ratios for various decays into $\chi^+\chi^-$ pairs. Note: this is the cross section for producing the mother particle times the branching ratio for the mother particle to decay into $\chi^+\chi^-$. Multiply by two to get the $\chi^\pm$ production cross section. For non-DY modes, the mother particle must be in $|\eta| < 2$, but the daughter $\chi^\pm$ could have $|\eta| > 2$. On the other hand some χs with $|\eta| < 2$ can arise from mothers of $|\eta| > 2$. For DY, it doesn't make sense to use "mother η" (it's almost always $\pm\infty$), so the plotted cross section requires at least one mCP to have $|\eta| < 1$. This threshold was chosen so that the probability of an mCP pointing in the vicinity of the detector is similar to that from the other non-DY production modes, in order to facilitate comparison. The plateau in DY cross section below $m_\chi = 1$ GeV is due to a 2 GeV $\chi^+\chi^-$ invariant mass cut in MadGraph.

6 Putting cross sections and BR together

The total cross section for milliCharged particle production (excluding DY) is shown in Fig. 8. As mentioned in Section 3, we are skipping $\eta' \to \pi^+\pi^-\chi^+\chi^-$. Note that the other contributions from η' in the plot are neglogible. Since for $\chi = e$ the branching ratio of the skipped process is four times higher than that of $\eta' \to e^+e^-\gamma$ (Dalitz decay), one worries that this process could actually be important. However, for reasonable χ masses, say above 100 MeV, this process is suppressed by phase space with respect to Dalitz decay, e.g., from the PDG, BR($\eta' \to \mu^+\mu^-\gamma$) $\approx$ 1e-4 while BR($\eta' \to \pi^+\pi^-\mu^+\mu^-$) < 3e-5. So we can safely ignore it.

As mentioned in the caption of Figure 8 some of the χs in the central region (i.e.: potentially within the acceptance of milliQan) could result from decays of mother particles at higher $|\eta|$, especially in the cases where the mother particles have low momentum and the
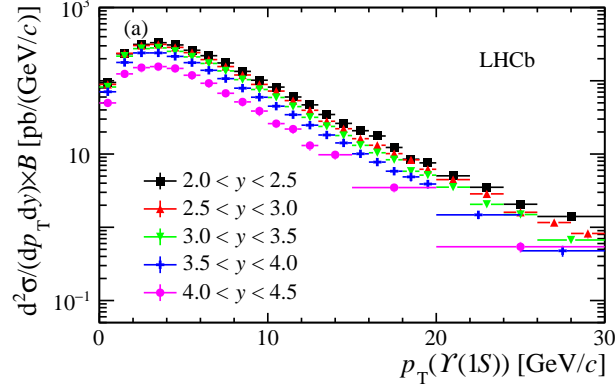
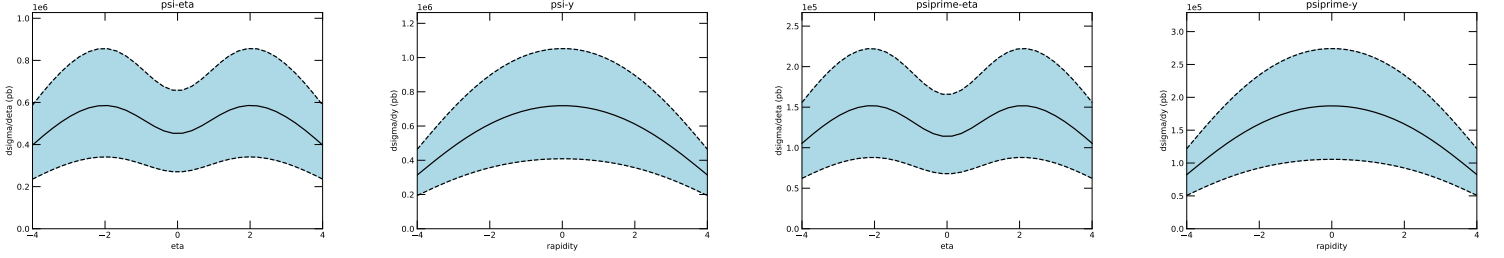Figure 9: $\Upsilon(1S)$ spectra in different rapidity ranges from LHCb [17].

Figure 10: Pseudorapidity and rapidity distributions from ψ (left) and $\psi(2S)$ (right) from b-decays[9, 10]. These are for $p_T < 10$ GeV, i.e., in the low boost regime. Note that in this p_T range the theoretical uncertainties are large.

boost in the decay is small. Particle production is nearly flat in rapidity, see Figures 9, 10 for some examples. The event generation will then assume a flat pseudorapidity distribution. At the analysis level one will be able to keep track of the contributions from high $|\eta|$ mothers, and assign a systematic if necessary.

7 Generation of the decays

We provide functions that take as input the lab frame 4-vector of either pseudoscalar (P) or vector (V) meson, and return the 4 vectors of the two χs from the decay. We assume that the V's are unpolarized.

7.1 Generation of pseudoscalar Dalitz decays

The implementation goes as follows (this also works for the Dalitz decay of the ω, whcih has J=1, as long as it is unpolarized):

- Rotate the 4-vector of P from the lab frame into frame S_1 such that P is traveling in the z-direction.

- Boost along z into frame S_2 where P is at rest.

- Pick a q^2 according to equation 1.

- Generate a decay $P \to X\gamma^*$ where γ^* is a particle of $m^2 = q^2$. The γ^* direction is random in ϕ and random in $\cos\theta$.

- Rotate the γ^* 4-vector into a frame S_3 such that the γ^* is traveling in the z-direction.

- Boost along z into frame S_4 where γ^* is at rest.

- Generate a decay $\gamma^* \to \chi^+\chi^-$ such that the angle ϕ of the χ^+ is random and $\cos\theta$ is picked according to [8]

$$\frac{dN}{d\cos\theta} = 1 + \cos^2\theta + \frac{4m_\chi^2}{q^2}\sin^2\theta \tag{6}$$

- Set the 3-vector of the χ^- to be back-to-back with the χ^+.

- Boost the 4-vectors of the χs from S_4 to S_3.

- Rotate the 4-vectors of the χs from S_3 to S_2.

- Boost the 4-vectors of the χs from S_2 to S_1.

- Rotate the 4-vectors of the χs from S_1 to the lab frame.

7.2 Generation of vector decays

The procedure is the following:

- Rotate the 4-vector of V from the lab frame into frame S_1 such that V is traveling in the z-direction.

- Boost along z into frame S_2 where V is at rest.

- Generate a decay $V \to \chi^+ \chi^-$ such that both the angle ϕ and the $\cos\theta$ of the χ^+ are random.

- Set the 3-vector of the χ^- to be back-to-back with the χ^+.

- Boost the 4-vectors of the χs from S_2 to S_1.

- Rotate the 4-vectors of the χs from S_1 to the lab frame.

References

[1] B. Holdom, Phys.Lett. B166, 196 (1986).

[2] A. Haas, C. S. Hill, E. Izaguirre and I. Yavin, Phys. Lett. B **746**, 117 (2015) doi:10.1016/j.physletb.2015.04.062 [arXiv:1410.6816 [hep-ph]].

[3] A. Ball *et al.*, arXiv:1607.04669 [physics.ins-det].

[4] L. G. Landsberg, Phys. Rep. 128, 301 (1985).

[5] See for example http://cds.cern.ch/record/683210/files/soft-96-032.pdf.

[6] Aloni, D., Efrati, A., Grossman, Y. et al. J. High Energ. Phys. (2017) 2017: 19.

[7] R. Van Royen and V. F. Weisskopf, Nuovo Cim. A 50, 617 (1967) Erratum: [Nuovo Cim. A 51, 583 (1967)].

[8] P. Adlarson et al., Phys. Rev. C 95, 025202 (2007).

[9] M. Cacciari, S. Frixione, N. Houdeau, M. L. Mangano, P. Nason and G. Ridolfi, JHEP **1210** (2012) 137 [arXiv:1205.6344 [hep-ph]].

[10] M. Cacciari, M. L. Mangano and P. Nason, arXiv:1507.06197 [hep-ph].

[11] V. Khachatryan *et al.* [CMS Collaboration], Phys. Rev. D **83**, 112004 (2011) doi:10.1103/PhysRevD.83.112004 [arXiv:1012.5545 [hep-ex]].

[12] S. Chatrchyan *et al.* [CMS Collaboration], Phys. Lett. B **727**, 101 (2013) doi:10.1016/j.physletb.2013.10.033 [arXiv:1303.5900 [hep-ex]].

[13] V. Khachatryan *et al.* [CMS Collaboration], Phys. Lett. B **749**, 14 (2015) doi:10.1016/j.physletb.2015.07.037 [arXiv:1501.07750 [hep-ex]].

[14] A. M. Sirunyan *et al.* [CMS Collaboration], Phys. Lett. B **780**, 251 (2018) doi:10.1016/j.physletb.2018.02.033 [arXiv:1710.11002 [hep-ex]].

[15] G. Aad *et al.* [ATLAS Collaboration], Phys. Lett. B **705** (2011) 9 doi:10.1016/j.physletb.2011.09.092 [arXiv:1106.5325 [hep-ex]].

[16] G. Aad *et al.* [ATLAS Collaboration], Phys. Rev. D **87**, no. 5, 052004 (2013) doi:10.1103/PhysRevD.87.052004 [arXiv:1211.7255 [hep-ex]].

[17] R. Aaij *et al.* [LHCb Collaboration], JHEP **1807** (2018) 134 Erratum: [JHEP **1905** (2019) 076] doi:10.1007/JHEP07(2018)134, 10.1007/JHEP05(2019)076 [arXiv:1804.09214 [hep-ex]].

[18] R. Aaij *et al.* [LHCb Collaboration], JHEP **1511** (2015) 103 doi:10.1007/JHEP11(2015)103 [arXiv:1509.02372 [hep-ex]].

[19] R. Aaij *et al.* [LHCb Collaboration], Eur. Phys. J. C **74** (2014) no.4, 2835 doi:10.1140/epjc/s10052-014-2835-1 [arXiv:1402.2539 [hep-ex]].

[20] R. Aaij *et al.* [LHCb Collaboration], JHEP **1306**, 064 (2013) doi:10.1007/JHEP06(2013)064 [arXiv:1304.6977 [hep-ex]].

[21] R. Aaij *et al.* [LHCb Collaboration], Eur. Phys. J. C **72**, 2025 (2012) doi:10.1140/epjc/s10052-012-2025-y [arXiv:1202.6579 [hep-ex]].

[22] H. Han, Y. Q. Ma, C. Meng, H. S. Shao, Y. J. Zhang and K. T. Chao, Phys. Rev. D **94**, no. 1, 014028 (2016) doi:10.1103/PhysRevD.94.014028 [arXiv:1410.8537 [hep-ph]].

[23] Y. Q. Ma, K. Wang and K. T. Chao, Phys. Rev. Lett. **106**, 042002 (2011) doi:10.1103/PhysRevLett.106.042002 [arXiv:1009.3655 [hep-ph]].

[24] Y. Q. Ma and R. Venugopalan, Phys. Rev. Lett. **113**, no. 19, 192301 (2014) doi:10.1103/PhysRevLett.113.192301 [arXiv:1408.4075 [hep-ph]].

[25] Y. Q. Ma, K. Wang and K. T. Chao, Phys. Rev. D **84**, 114001 (2011) doi:10.1103/PhysRevD.84.114001 [arXiv:1012.1030 [hep-ph]].

[26] V. Khachatryan *et al.* [CMS Collaboration], Eur. Phys. J. C **71**, 1575 (2011) doi:10.1140/epjc/s10052-011-1575-8 [arXiv:1011.4193 [hep-ex]].

[27] A. M. Sirunyan *et al.* [CMS Collaboration], Phys. Rev. D **96**, no. 11, 112003 (2017) doi:10.1103/PhysRevD.96.112003 [arXiv:1706.10194 [hep-ex]].

[28] http://home.thep.lu.se/~torbjorn/pythia81php/Welcome.php. Click on QCD on the left panel.

[29] M. Aaboud *et al.* [ATLAS Collaboration], Phys. Rev. Lett. **117** (2016) 182002 doi:10.1103/PhysRevLett.117.182002 [arXiv:1606.02625 [hep-ex]].

[30] CMS Collaboration, CMS-PAS-FSQ-15-005.

[31] S. Acharya *et al.* [ALICE Collaboration], Eur. Phys. J. C (2018) 78: 263. doi:10.1140/epjc/s10052-018-5612-8 [arXiv:1708.08745 [hep-ex]].

[32] P. Skands, S. Carrazza, and J. Rojo, Eur. Phys. J. C (2014) 3024. [arXiv:1404.5630 [hep-ph]].

[33] S. Acharya *et al.* [ALICE Collaboration], Phys. Rev. C **99** (2019), 064901. doi:10.1103/PhysRevC.99.064901 [arXiv:1805.04365 [hep-ex]].

[34] ALICE Collaboration, ALICE-PUBLIC-2018-004.

[35] G. Aad *et al.* [ATLAS Collaboration], Eur. Phys. J. C (2014) 74: 2895. doi:10.1140/epjc/s10052-014-2895-2 [arXiv:1402.6162 [hep-ex]].

[36] M. Albrow *et al.* (TeV4 QCD Working Group), [arXiv:0610012 [hep-ph]]. Fermilab-Conf-06-359.